

WildAvatar: Web-scale In-the-wild Video Dataset for 3D Avatar Creation

Zihao Huang¹, Shoukang Hu², Guangcong Wang³, Tianqi Liu¹,
Yuhang Zang⁴, Zhiguo Cao¹, Wei Li^{2,†}, Ziwei Liu²

¹Huazhong University of Science and Technology, ²S-Lab, Nanyang Technological University,
³Great Bay University, ⁴Shanghai AI Laboratory

<https://wildavatar.github.io/>



Figure 1: Examples from our WildAvatar dataset. Unlike previous laboratory datasets for 3D avatar creation, WildAvatar curates in-the-wild web videos. With 10,000+ human subjects and scenes, WildAvatar is at least $10\times$ richer than the previous datasets, covering a wide range of real-world human motions and appearances. It contains high-quality annotations (*i.e.*, SMPL, camera parameters, and human segmentation masks).

Abstract

Existing human datasets for avatar creation are typically limited to laboratory environments, wherein high-quality annotations (*e.g.*, SMPL estimation from 3D scans or multi-view images) can be ideally provided. However, their annotating requirements are impractical for real-world images or videos, posing challenges toward real-world applications on current avatar creation methods. To this end, we propose the **WildAvatar** dataset, a web-scale in-the-wild human avatar creation dataset extracted from YouTube, with 10,000+ different human subjects and scenes. WildAvatar is at least $10\times$ richer than previous datasets for 3D human avatar creation. We evaluate several state-of-the-art avatar creation methods on our dataset, highlighting the unexplored challenges in real-world applications on avatar creation. We also demonstrate the potential for generalizability of avatar creation methods, when provided with data at scale. We publicly release our data source links and annotations, to push forward 3D human avatar creation and other related fields for real-world applications.

1 Introduction

3D Human Avatar creation has extensive applications in VR/AR, film-making, metaverse, *etc.*, attracting significant attention recently. With the advent of neural radiance fields (NeRF) [49, 66],

Table 1: Statistics on different human datasets for avatar creation. We only consider human datasets that include human appearances. : multi-camera system. : 3D scanner. : depth sensor. : inertial measurement unit. : professional actor. Our WildAvatar is a *large-scale* and *in-the-wild* avatar dataset collected with our designed *automatic collection* pipeline.

Dataset	#Sub./Sce.	Type	Cost	Dataset	#Sub./Sce.	Type	Cost
ZJU-Mocap [53]	9/6	Lab	+	RenderPeople [56]	482/—	Lab	+
HuMMan [9]	339/20	Lab	++	THuman [84]	100/10	Lab	+
DyMVHumans [82]	32/45	Lab	+	THuman2.0 [78]	500/—	Lab	++
Human3.6M [28]	11/15	Lab	++	THuman3.0 [63]	20/—	Lab	++
THuman4.0 [83]	3/3	Lab	+	THuman5.0 [62]	10/10	Lab	+
Hi4D [76]	40/10	Lab	++	DNA [14]	500/1187	Lab	++
DynaCap [21]	4/5	Lab	+	MultiHuman [81]	50/—	Lab	+
UltraStage [85]	100/20	Lab	+	Actors-HQ [29]	8/21	Lab	+
HUMBI [77]	772/4	Lab	+	NHR [73]	4/3	Lab	+
AIST++ [67]	30/10	Lab	+	MPII [5]	8/1	Lab	+
ENeRF [42]	7/4	ITW	+	3DPW [68]	7/4	ITW	++
FreeMan [69]	40/123	ITW	+	SynWild [20]	5/5	ITW	—
NeuMan [31]	6/6	ITW	—	TikTok [30]	340/340	ITW	—
IVS-Net [15]	<700/<700	ITW	—	<i>WildAvatar</i>	10k+/10k+	ITW	—

recent research aims to recover 3D avatars from 2D observations, enabling the synthesis of novel images from arbitrary viewpoints and body poses [72, 53, 51, 26, 18, 38, 25]. For example, many works focus on reconstructing animatable human models from well-annotated and calibrated multi-view images and videos [53, 51, 52, 73], and have achieved photo-realistic results in laboratory datasets [53, 56, 4]. However, the well-designed collection systems limit its scalability to real-world scenes. To mitigate the gap between the ideal laboratory setting and real-world scenarios, a line of research proposes to reconstruct human avatars from monocular videos [19, 26, 72] or even a single image [25, 15], considering these forms of data can be easily accessible in our daily life. Still, these methods require annotations from multi-view images or even 3D scans. In addition, their performances are restricted by small-scale human data, especially for generalizable creation.

Although previous arts attempted to make existing laboratory datasets more suitable for real-world applications, there still exists a domain gap between laboratory and real-world scenarios. This is down to the fact that current human datasets are mainly collected via well-designed laboratory systems, which are expensive and time-consuming to collect. As shown in Tab. 1, existing human data collections mostly rely on accurate annotations from various advanced devices, such as well-calibrated multi-view cameras [78, 63, 48, 14], depth sensors [9, 84, 78, 28], IMUs [68], or expensive scanners [56, 76], as well as specialized actors and lightstages [21, 77, 67, 69, 42]. This ideal condition is unavailable in in-the-wild scenarios (*i.e.*, monocular web videos) or consumer applications. To tackle this problem, recent efforts are attempting to collect in-the-wild monocular human data [30, 15, 17] but rely heavily on costly manual interventions, making it difficult to scale up. Therefore, their inadequate diversity fails to meet the requirements for dealing with in-the-wild challenges of 3D avatar creation. Given the shortage of in-the-wild human data, scaling up avatar creation from real-world scenarios is worth exploring.

To facilitate the in-the-wild avatar creation, we curate WildAvatar, a large-scale in-the-wild human avatar creation dataset extracted from YouTube, with 10,000+ different human subjects and scenes. Specifically, we collect monocular human videos from YouTube and streamline the annotation process with off-the-shelf state-of-the-art annotation methods [55, 36, 2, 34], *e.g.*, YOLO [55], Segment Anything [34]. Without costly sensors or lightstages, we collect over 10,000 in-the-wild human samples. WildAvatar fills the gap in large-scale in-the-wild human data collection, offering at least $10\times$ richer human subjects than the existing human datasets.

To investigate the performance of existing avatar creation methods in real-world scenarios, we evaluate state-of-the-art avatar creation methods [53, 51, 72, 26] on our WildAvatar dataset. Compared to laboratory datasets, existing methods encounter a significant performance drop in the reconstruction quality of the WildAvatar dataset. This highlights the gap between well-annotated laboratory datasets and in-the-wild datasets for avatar creation. We also investigate the scalability of existing

generalizable human avatar creation methods [18, 38, 25] with WildAvatar, which suggests a significant improvement (up to 7%) in real-world scenarios. We will release the WildAvatar dataset, providing the video IDs, frame IDs, extracting scripts, and annotations obtained from our pipeline. We hope that our dataset will push forward the development of 3D human avatar creation, and other related topics, *e.g.*, human mesh estimation (HPS) [33, 36, 41, 79, 37, 35, 27] and 3D human avatar generation [10, 23, 12, 24, 70, 46]. Overall, our main contributions are summarized as follows:

- We present WildAvatar, a large-scale avatar dataset collected from in-the-wild videos with more than 10,000 human subjects, at least $10\times$ larger than previous datasets. The scale-up facilitates the creation of per-subject human avatars and paves a new avenue for generalizable human avatar reconstruction.
- We evaluate the performance of existing state-of-the-art human avatar creation methods on the collected WildAvatar, showing the critical challenges of the in-the-wild avatar creation. Our observations could inspire the key directions in the human avatar creation.
- We will release our data collection and annotation pipeline for WildAvatar. Further data scale-up for large-scale model training will be unlocked. The open data and code could provide important insights for future avatar creation and relevant human generation models.

2 Related Work

3D Avatar Creation Datasets. Tab. 1 presents a system overview of previous avatar creation datasets. Previous datasets mainly obtain high-quality human mask and SMPL annotations with ideal laboratory systems, *e.g.*, well-calibrated multi-view cameras [53, 9, 82, 78, 28, 63, 83, 62, 76, 14, 21, 81, 85, 29, 77, 73, 67, 48, 42, 68], depth sensors [9, 84, 78, 28, 63, 14], IMUs [68], or expensive scanners [56, 76], as well as specialized actors and lightstages [53, 56, 9, 84, 82, 78, 28, 63, 83, 62, 76, 14, 21, 81, 85, 29, 77, 73, 67, 48, 42, 68], depth sensors [9, 84, 78, 28, 63, 14]. Unfortunately, in real-world scenarios or applications, these optimal conditions are typically hard to guarantee. Towards in-the-wild avatar creation, previous efforts also attempt to collect web human videos [30, 15]. However, they rely heavily on costly manual interventions (*e.g.*, pre-screening or mask extraction based for [44]) and fail to scale up. And they either show little viewpoint change [30] or not public released [15]. Therefore, there are still significant demands for a public large-scale in-the-wild dataset for avatar creation.

3D Avatar Creation Methods. Existing works on avatar creation learn coarse human surfaces with parametric mesh models [6, 47, 50, 74, 57], but these explicit meshes cannot express detailed geometry or appearance. Pifu-based methods [58, 59, 22, 40, 16] represent the human body with pixel-aligned functions and require high-quality synthetic data, but fail to generalize to real-world scenarios due to the domain gap. NeRF-based approaches [53, 51, 72, 52, 19, 39, 8, 75] learn implicit human representation from high-quality videos, and achieve photo-realistic rendering in the laboratory benchmarks. In addition, generalizable models [18, 38, 25] further simplify the data demand to a single image. Nonetheless, these methods still rely on accurate annotations, which only exist in ideal laboratory environments. Recent attempts [31, 20] decompose avatars and scenes for construction at once, demanding accurate global alignments between human bodies and backgrounds that are not available in real-world videos.

SMPL Estimation in the Wild. Parametric body models (*e.g.*, SMPL [47], SMPLX [50]) encode coarse human surfaces with pose and shape parameters for avatar creation. For example, end-to-end methods [33, 36, 79, 41, 27] estimate the SMPL parameters efficiently from a single in-the-wild image, but they are not robust with complex scenes. Subsequent works [37, 32] refine end-to-end estimation results via fitting SMPL to 2D annotations in the loop. Recent works further consider imposing temporal consistency [2, 65, 35] to smooth SMPL estimations across input in-the-wild videos. Yet, it is far from a comprehensive annotating streamline for real-world video sources.

3 WildAvatar

Our goal is to build a large-scale in-the-wild dataset for human avatar creation. To this end, we collect abundant real-world human videos from YouTube and annotate corresponding labels. Without time-consuming and high-cost manual filtering and annotation [15], we design an efficient pipeline

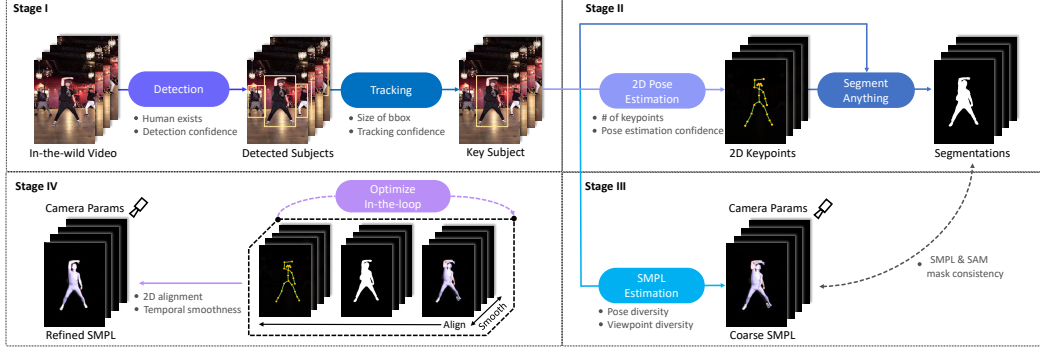


Figure 2: The four-stage data processing pipeline. We first obtain the bounding box of key subjects in videos in Stage I and extract human segmentation masks in Stage II. Then the SMPL and camera parameters are coarsely estimated in Stage III and later refined in Stage IV.

to filter video candidates and obtain high-quality annotations. Specifically, we download human movement web videos with our automatic pipeline, as described in Sec. 3.1. Then, as described in Sec. 3.2, we perform several processing steps (*e.g.*, filtering and annotation) on downloaded web videos. We collect a dataset of $10k+$ real-world human videos with $200k+$ frames and annotations.

3.1 Data Collection

We follow two steps to collect human movement videos: 1) We first search for a large diverse set of video candidates on YouTube. Note that video candidates could contain some noisy videos without human movement; 2) We then download candidate videos with automatic tools [3], cut them into clips, and filter out short video clips.

Downloading Video Candidates. To cover a wide range of in-the-wild human-central activities, we start from a label pool of human motion datasets [43]. Based on these human motion labels (*e.g.*, fishing and playing tennis), we download over $100k$ video candidates from YouTube API.

Filtering Video Clips. Some collected video candidates could not meet the high-quality human avatar creation requirement. For example, human bodies may not exist (*e.g.*, preview, occlusion) or frequently change poses (*e.g.*, montage) in some frames of these videos. To filter out such videos, we cut video candidates into clips with SceneDetect [1] and discard video candidates with only short clips. After filtering video candidates, we obtain $460k$ video clip candidates for further processing.

3.2 Data Processing

To obtain high-quality annotations (*i.e.*, SMPL, camera parameters, and human segmentation mask) for collected human videos, we adopt the following four stages to annotate human video clips.

Stage I: Human Bounding Box Detection and Tracking. Precise human bounding boxes are important for monocular SMPL estimation methods [36, 33, 41, 79] and human segmentation (using *Segment Anything* [34]). Hence, we first obtain the bounding box of human subjects with an off-the-shelf state-of-the-art Yolo detection method [55]. Then we filter out video clip candidates with either short (*e.g.*, less than 2 seconds) human activity sequences or low detection or tracking confidence. Finally, we only keep the tracked subject with the largest bounding box on average (*i.e.*, key subject) over the whole video clip sequence.

Stage II: Human Segmentation Mask Extraction. Foreground segmentation masks that distinguish human subjects from the background are important for 3D avatar creation. Previous methods [15, 72] adopt the *background matting* [44] methods for segmentation. These methods, however, require manual intervention to select the collected videos with at least one still background image, which is time-consuming to prepare. To efficiently segment human video clips, we adopt state-of-the-art *Segment Anything* (SAM) [34], which only requires bounding boxes and key points for each frame obtained in previous human detection, tracking, and 2D pose estimation steps (See Fig. 2).

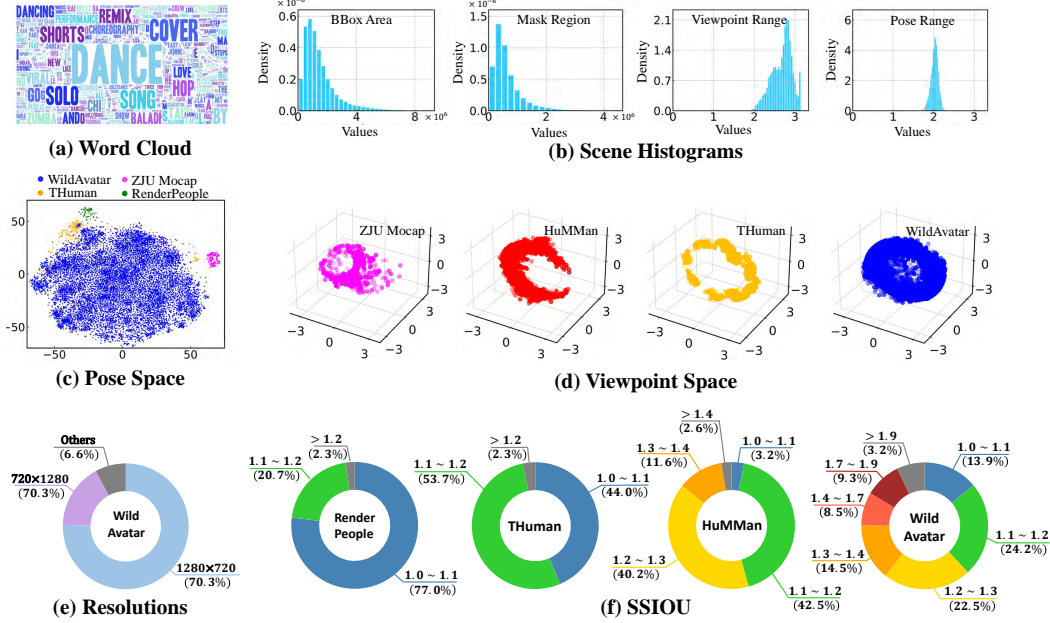


Figure 3: Data Analysis: (a) word cloud of the video titles in WildAvatar, (b) histograms of annotations across video clips, here we count the bounding box and human mask region in pixels, and “Range” denotes the difference between the maximum and minimum values. (c) comparison of the body pose spaces with popular laboratory human datasets, (d) comparison of the viewpoints spaces with popular laboratory human datasets, (e) resolutions of videos in WildAvatar, and (f) comparison with the previous dataset on the abundance of clothing. We introduce the SSIU, the inverse IOU between SMPL [47, 50] masks and segmentation masks.

Stage III: Coarse SMPL and Camera Estimation. We first estimate SMPL and camera parameters frame by frame, using a state-of-the-art single-image-based human pose and shape estimation method PARE [36]. Then, we check the pose and viewpoint shifts of the remaining video clips and only retain those with considerable viewpoint shifts and human movements. The estimated coarse SMPL and camera parameters will be used as initialization for implicit human reconstruction methods [72, 53, 51] to further refine SMPL and camera parameters in Stage IV.

Due to the depth ambiguity, monocular SMPL estimation and SAM might have low overlaps in estimated human masks. We double-check their consistency by comparing SMPL projection masks with the SAM masks. Intuitively, the SMPL mask denotes the naked body, while the SAM mask contains the clothed body. Therefore, the SMPL mask should be mostly covered by the SAM mask. To guarantee high-quality annotations, we discard video clips whose SAM-masked region has small overlaps with the SMPL-masked region.

Stage IV: Refining SMPL and Camera In-the-loop. The coarse SMPL estimated in Stage I may ignore the temporal consistency of human motions. Inspired by previous SMPL annotation pipelines [37, 2, 32], we further refine SMPL and camera parameters by smoothing these parameters across the whole video clip sequence via gradient descent. We also incorporate the estimated 2D keypoints and SAM masks into a refinement loop, providing additional supervision for precise SMPL and camera parameter estimation. Qualitative comparisons between coarse and refined SMPL and camera parameters can be found in the Fig. A1.

3.3 Data Analysis

Our collected WildAvatar contains 10,647 real-world human video clips with 200k+ images. We randomly split WildAvatar into training, validation, and test splits with 7k, 1.5k, and 1.5k subjects, respectively. We show data statistics of our WildAvatar in Fig. 3 and describe the details of pose, viewpoint, and clothing distribution as follows.

Poses: Various vs. Tedious. In Fig. 3 (c), we compare the pose distribution differences among WildAvatar and previous human datasets. Specifically, we visualize the top-2 components of body

Table 2: Quantitative comparisons on WildAvatar benchmark. We report the quality of novel pose synthesis of popular methods, on both the lab benchmark ZJU-Mocap and our WildAvatar.

Method	Train	FPS	WildAvatar			ZJU-Mocap		
			PSNR \uparrow	SSIM \uparrow	LPIPS \downarrow	PSNR \uparrow	SSIM \uparrow	LPIPS \downarrow
NHR [73]	5h	1.23	18.72	91.1	10.1	28.25	89.2	12.2
NeuralBody [53]	10h	1.48	16.55	85.8	12.6	30.66	96.4	4.3
Animatable NeRF [51]	10h	1.11	19.43	91.0	10.4	29.77	96.5	4.7
Animatable SDF [52]	10h	0.40	19.20	91.9	11.4	30.38	97.5	3.7
HumanNeRF [72]	10h	0.30	22.65	87.1	15.4	30.66	96.9	3.3
InstantNVR [19]	5m	2.20	23.01	91.9	9.9	31.01	97.1	3.8
GauHuman [26]	1m	189	24.02	92.1	9.1	31.34	96.5	3.1

poses with t-SNE [54] dimension reduction. The pose distribution comparison shows that our WildAvatar contains more diverse poses than previous laboratory datasets, as laboratory datasets only contain several designed motion sequences. This illustrates the importance of our large-scale in-the-wild WildAvatar when applying the existing models to real-world scenarios.

Viewpoints: Free vs. Fixed. We compare viewpoint distribution among previous human datasets [53, 9, 84] and WildAvatar. Specifically, we visualize the 3D rotations of observed cameras relative to human subjects. As suggested in Tab. 1, previous laboratory datasets are mainly collected in indoor lightstages, where the RGB(D) cameras’ positions are fixed for whole datasets. In real-world scenarios, however, the viewpoints of humans are arbitrary. As shown in Fig. 3 (d), the viewpoint distributions in previous datasets are sparse or unbalanced, while our WildAvatar covers a more dense viewpoint distribution.

Cloth: Diversity vs. Unitary. Previous laboratory human datasets mainly contain unitary tight clothes, while complex real-world appearances (e.g., different hairstyles) and diverse loose clothes are seldom involved. Our WildAvatar involves diverse tight and loose clothes in the real world. To quantitatively measure the clothing diversity between real-world and laboratory data, we define a metric (SSIOU) that calculates the inverse IOU between SMPL [47, 50] projected masks and human segmentation masks among different datasets in Fig. 3 (f). For humans with tight clothes, the measured SSIOU is close to 1.0 (blue in Fig. 3 (f)), indicating their SMPL masks are similar to human segmentation masks. Correspondingly, a larger SSIOU (red in Fig. 3 (f)) reveals that human clothes are looser, with segmentation masks being larger than SMPL masks. As shown in Fig. 3 (f), more than 30% subjects in WildAvatar have SSIOU values over 1.4, suggesting that WildAvatar covers various types of clothes. This analysis validates that WildAvatar satisfies data distributions in real-world scenarios.

4 Experiments

We evaluate previous state-of-the-art methods on our WildAvatar dataset with the following commonly used metrics (details in Sec. 4.1) on 3D avatar creation. To illustrate the unclaimed challenges for avatar creation in the wild, we benchmark previous popular per-subject methods in Sec. 4.2. To further demonstrate the benefit of the large-scale WildAvatar, we compare generalizable avatar creation methods in Sec. 4.3.

4.1 Evaluation Metrics

To quantitatively evaluate the quality of novel view and novel pose synthesis, we apply three commonly used metrics: peak signal-to-noise ratio (PSNR) [60], structural similarity index (SSIM) [71], and Learned Perceptual Image Patch Similarity (LPIPS) [80]. Following previous literature [38, 25], we compute whole-image metrics for per-subject reconstruction methods, while reporting the metrics based on projected 3D human bounding box areas for generalizable methods.

4.2 Track A: Per-Subject Human Avatar Creation

Setup. To explore the quality of WildAvatar and investigate the maximum reconstruction performance on monocular in-the-wild videos. We evaluate popular per-subject avatar creation methods on our WildAvatar dataset. We evaluate a total of 7 baselines: Neural Human Rendering (NHR) [73],

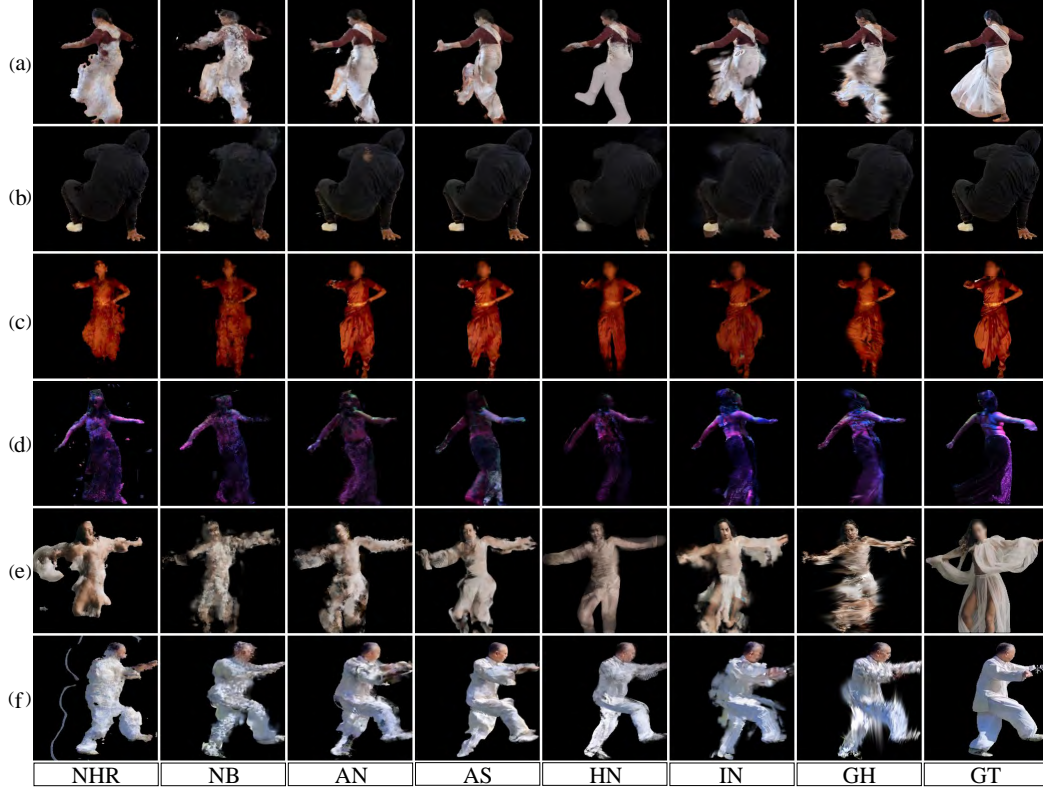


Figure 4: Qualitative comparisons of popular per-subject methods on WildAvatar. NHR and NB, AN, AS, HN, IN, and GH denote Neural Human Rendering, NeuralBody, Animatable NeRF, Animatable SDF, HumanNeRF, InstantNVR, and GauHuman, respectively. Faces are blurred to protect privacy.

NeuralBody (NB) [53], Animatable NeRF (AN) [51], Animatable SDF (AS) [52], HumanNeRF (HN) [72], InstantNVR (IN) [19], and GauHuman (GH) [26]. Considering the calculating and time cost, it is impractical and inefficient to train all scenes in WildAvatar. Instead, we manually select 10 representative human subjects from WildAvatar for benchmarking. For each subject, we randomly choose 10 frames for training and the remaining 10 frames are for testing. We follow the default model settings (learning rate, batch size, *etc.*) in official implementations and report average metrics of these baselines in Tab. 2.

Quantitative and Qualitative Analysis. As shown in Tab. 2, existing methods struggle to handle the more challenging in-the-wild WildAvatar, resulting in unsatisfactory performance. Compared to the popular ZJU Mocap [53] benchmark, there is a marginal drop of PSNR (-10.12), SSIM (-8.04), and LPIPS ($+6.47$) on average. We further present qualitative comparisons in Fig. 4, and outline three potential challenges towards in-the-wild avatar creation in the following.

Noisy Annotation. The quality of avatar creation significantly depends on the quality of annotations. Although we streamline our annotation pipeline with the best existing methods, it is unrealistic to annotate in-the-wild scenarios as accurately as in the lab. Specifically, existing monocular SMPL estimation methods may fail in challenging areas (*e.g.*, hands and feet), and segmentation methods may also convey unstable artifacts (See GT in Fig. 4 (f)). It is an imperative field that investigates methods for reconstructing the human body from noisy in-the-wild data.

Loose Cloth. In-the-wild data features a wide variety of clothing, rather than dominant tight garments (*e.g.*, T-shirts and shorts) in existing laboratory datasets. These loose clothes introduce non-rigid motions and ambiguous deformation weights, which pose significant challenges for avatar creation methods. As shown in Fig. 4 (a), (e), and (f), existing methods struggle to reconstruct loose garments and are prone to render fuzzy or floating regions. These garments are positional ambiguous to render in novel poses, as they are not considered in the existing body models [47, 50].

Table 3: Generalizability comparisons on challenging WildAvatar and laboratory benchmarks. We report the results of previous generalizable avatar creation methods on the cross-domain setting. NP/NV denotes Novel Pose/View. RP/THU/HM/ZJU/WA are short for RenderPeople [56] / THuman [84] / HuMMan [9] / ZJU Mocap [53] / WildAvatar (Ours) dataset. Novel Lab Test refers to the test split of laboratory datasets not included in the training.

Method	Training Set					WildAvatar Test			Novel Lab Test	
	WA	RP	THU	HM	ZJU	PSNR(NP)	SSIM(NP)	LPIPS(NP)	PSNR(NV)	PSNR(NP)
NHP [18]	✓		✓	✓	✓	17.39	62.6	33.2	20.05	19.83
			✓	✓	✓	18.12	66.3	31.4	20.49	20.24
		✓		✓	✓	17.35	62.2	33.4	20.84	20.81
		✓		✓	✓	18.07	66.9	31.2	21.20	21.27
MPS-NeRF [38]	✓	✓	✓		✓	18.21	74.2	24.0	18.46	18.76
		✓	✓		✓	18.79	76.8	22.2	18.48	18.77
		✓	✓	✓		18.20	74.3	23.8	21.15	21.43
		✓	✓	✓		19.11	77.2	22.1	21.19	21.48
SHERF [25]	✓		✓	✓	✓	18.39	78.1	20.2	20.67	20.10
			✓	✓	✓	19.43	80.5	19.3	20.96	20.49
		✓	✓		✓	18.31	77.9	20.4	19.07	18.99
		✓	✓		✓	19.50	80.7	19.2	19.63	19.73
Generalizable GS	✓	✓		✓	✓	17.76	81.1	22.8	20.31	20.03
		✓		✓	✓	18.43	81.5	22.3	21.73	21.65
		✓	✓	✓		17.73	81.2	22.7	21.47	21.78
		✓	✓	✓		18.39	81.4	22.4	22.46	22.02

Uneven Light Condition. Most state-of-the-art methods [51, 72, 26, 53] reconstruct avatars only in the canonical space, and they warp the space from canonical to observation in novel pose synthesis. This fashion assumes a uniformity of light distribution of the target scenes, which is easy to set up in laboratory lightstages. However, real-world scenarios are usually illuminated in partial-occluded directions. This uneven light condition makes it more challenging to learn diffuse-aware avatars from monocular videos. Current avatar reconstruction models struggle to distinguish the reflection effects and cloth textures. This ambiguity may lead to dissonant lighting effects, *e.g.*, the dress region in Fig. 4 (d) and legs in Fig. 4 (f).

4.3 Track B: Generalizable Human Avatar Creation

Setup. We evaluate four state-of-the-art generalizable baselines on our large-scale WildAvatar, including 1) Neural Human Performer (NHP) [18], 2) MPS-NeRF [38], 3) SHERF [25], and 4) Generalizable 3D Gaussian Splatting (Generalizable GS). Specifically, the Generalizable GS is adapted from GauHuman [26], with the Gaussians’ attributes decoded from the input features, following the approaches in [11, 45]. To evaluate the overall generalizability among various scenarios, we also report results on four laboratory datasets, including 1) ZJU-Mocap [53], 2) RenderPeople [56], 3) HuMMan [9], and 4) THuman [84]. We split these datasets into training and test sets as in SHERF [25]. To avoid overfitting to a small indoor dataset, we adopt the cross-domain testing strategy, *e.g.* we mask out the ZJU training set when testing on the ZJU.

Quantitative and Qualitative Analysis. There are three main observations in Tab. 3. First, large-scale WildAvatar is essential for improving generalizability towards in-the-wild scenarios. Comparing odd and even rows, the WildAvatar training set brings considerable improvements in real-world scenarios. On the WildAvatar test set, it improves PSNR, SSIM, and LPIPS by 4.52%, 3.53%, and 5.06% on average, respectively. This suggests that using large-scale in-the-wild data is important for the generalizable avatar creation methods. As shown in Fig. 5, models without (w/o) training on WildAvatar, tend to predict dark-colored artifacts on the lower body. And models with (w/) training on WildAvatar can provide more realistic appearances. Second, large-scale in-the-wild data is also beneficial for laboratory benchmarks, although there are large domain gaps and the annotation of in-the-wild data is not as accurate as in the laboratory. By introducing WildAvatar dataset, we obtain an improvement of 2.57% and 2.50% PSNR on novel view and pose synthesis, respectively. Third, although 3D Gaussian Splatting (3DGS) performs well in per-subject human avatar creation, it shows

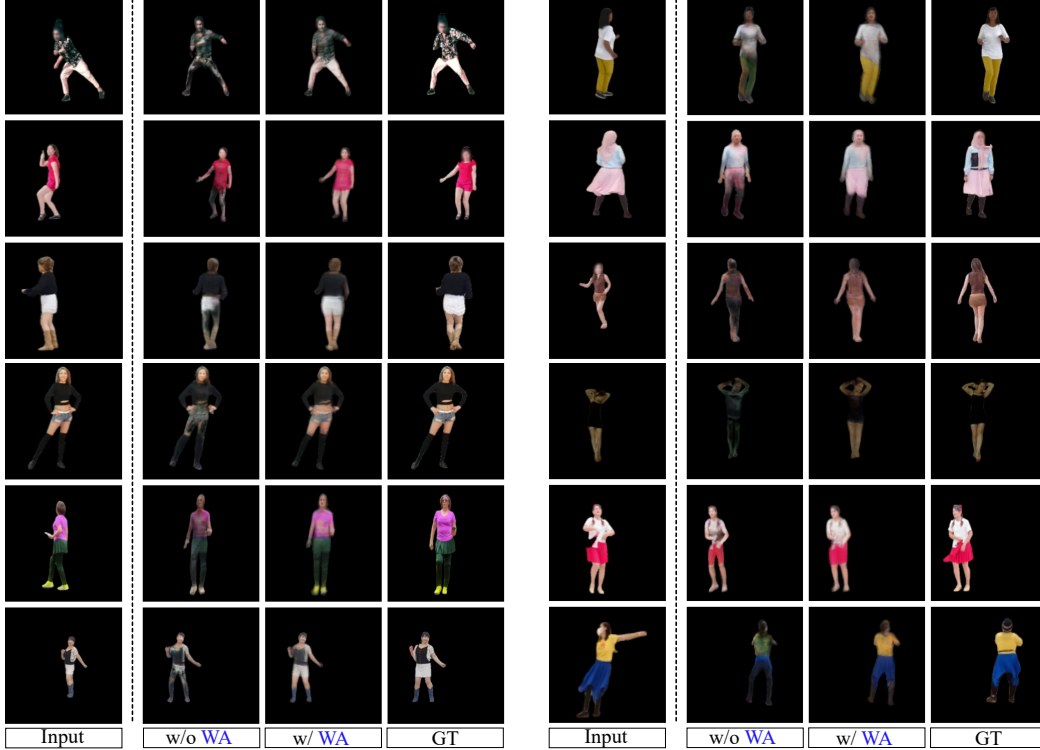


Figure 5: Qualitative comparisons on the state-of-the-art generalizable avatar creation method [25]. “w/ WA” or “w/o WA” denotes training with or without WildAvatar, respectively. Faces are blurred to protect privacy.

slightly worse than NeRF in this generalizable setting. Our insight is that 3DGS highly relies on the point cloud initialization [26, 13, 45]. Unfortunately, due to the depth ambiguity, it is challenging to infer accurate point cloud initialization from a single image.

5 Conclusions

We curate WildAvatar, a large-scale in-the-wild human avatar creation dataset from YouTube, with 10, 000+ various human subjects and scenes. Compared with traditional avatar creation datasets, our WildAvatar consists of at least $10\times$ more subjects or scenes. We benchmark state-of-the-art human avatar creation methods on WildAvatar, illuminate the potential of the avatar creation task with data at scale, and reveal its remaining challenges towards real-world applications. We hope this dataset will shed insights on following in-the-wild human avatar creation methods, and benefit 3D/4D human content generation works.

Pipeline Efficiency. The efficiency of data collection and annotation is also crucial to facilitate data scale-up and application. Despite the complex multiple-stage design, our data-collecting pipeline only takes less than 200 seconds to generate full annotations for an arbitrary in-the-wild video.

Limitations. Despite the advantages of WildAvatar, we would like to list several limitations: 1) WildAvatar focuses on the 3D modeling of human bodies, lacking the 3D information of background environments. 2) To meet the needs of the avatar creation, WildAvatar contains video scenes involving dynamic human motions. Human poses in static activities (*e.g.*, reading, fishing) are rarely included. 3) Multi-human interactions within the identical scenes are not covered.

Societal Impacts. In-the-wild avatar creations could enable potentially harmful uses. For instance, the unauthorized creation of avatars may violate portrait rights. Additionally, models trained on WildAvatar might exhibit biases in YouTube videos. Users should consider this when deploying, analyzing, and developing these models.

References

- [1] Video scene cut detection and analysis tool. Github, 2014.
- [2] Easymocap - make human motion capture easier. Github, 2021.
- [3] A feature-rich command-line audio/video downloader. Github, 2021.
- [4] Thiemo Alldieck, Marcus A. Magnor, Weipeng Xu, Christian Theobalt, and Gerard Pons-Moll. Video based reconstruction of 3d people models. In *2018 IEEE Conference on Computer Vision and Pattern Recognition, CVPR 2018, Salt Lake City, UT, USA, June 18-22, 2018*, pages 8387–8397. Computer Vision Foundation / IEEE Computer Society, 2018.
- [5] Mykhaylo Andriluka, Leonid Pishchulin, Peter V. Gehler, and Bernt Schiele. 2d human pose estimation: New benchmark and state of the art analysis. In *Proc. IEEE Conf. Comput. Vis. Patt. Recogn.*, pages 3686–3693. Computer Vision Foundation / IEEE, 2014.
- [6] Dragomir Anguelov, Praveen Srinivasan, Daphne Koller, Sebastian Thrun, Jim Rodgers, and James Davis. SCAPE: shape completion and animation of people. *ACM Trans. Graph.*, 24(3):408–416, 2005.
- [7] Federica Bogo, Angjoo Kanazawa, Christoph Lassner, Peter V. Gehler, Javier Romero, and Michael J. Black. Keep it SMPL: automatic estimation of 3d human pose and shape from a single image. In Bastian Leibe, Jiri Matas, Nicu Sebe, and Max Welling, editors, *Proc. Eur. Conf. Comput. Vis.*, volume 9909 of *Lecture Notes in Computer Science*, pages 561–578. Springer-Verlag, 2016.
- [8] Aljaz Bozic, Pablo R. Palafox, Michael Zollhöfer, Justus Thies, Angela Dai, and Matthias Nießner. Neural deformation graphs for globally-consistent non-rigid reconstruction. In *IEEE Conference on Computer Vision and Pattern Recognition, CVPR 2021, virtual, June 19-25, 2021*, pages 1450–1459. Computer Vision Foundation / IEEE, 2021.
- [9] Zhongang Cai, Daxuan Ren, Ailing Zeng, Zhengyu Lin, Tao Yu, Wenjia Wang, Xiangyu Fan, Yang Gao, Yifan Yu, Liang Pan, Fangzhou Hong, Mingyuan Zhang, Chen Change Loy, Lei Yang, and Ziwei Liu. Humman: Multi-modal 4d human dataset for versatile sensing and modeling. In Shai Avidan, Gabriel J. Brostow, Moustapha Cissé, Giovanni Maria Farinella, and Tal Hassner, editors, *Computer Vision - ECCV 2022 - 17th European Conference, Tel Aviv, Israel, October 23-27, 2022, Proceedings, Part VII*, volume 13667 of *Lecture Notes in Computer Science*, pages 557–577. Springer, 2022.
- [10] Eric R Chan, Connor Z Lin, Matthew A Chan, Koki Nagano, Boxiao Pan, Shalini De Mello, Orazio Gallo, Leonidas J Guibas, Jonathan Tremblay, Sameh Khamis, et al. Efficient geometry-aware 3d generative adversarial networks. In *Proceedings of the IEEE/CVF conference on computer vision and pattern recognition*, pages 16123–16133, 2022.
- [11] David Charatan, Sizhe Li, Andrea Tagliasacchi, and Vincent Sitzmann. pixelsplat: 3d gaussian splats from image pairs for scalable generalizable 3d reconstruction. In *arXiv*, 2023.
- [12] Zhaoxi Chen, Fangzhou Hong, Haiyi Mei, Guangcong Wang, Lei Yang, and Ziwei Liu. Primdiffusion: Volumetric primitives diffusion for 3d human generation. *Advances in Neural Information Processing Systems*, 36:13664–13677, 2023.
- [13] Kai Cheng, Xiaoxiao Long, Kaizhi Yang, Yao Yao, Wei Yin, Yuexin Ma, Wenping Wang, and Xuejin Chen. Gaussianpro: 3d gaussian splatting with progressive propagation. *arXiv preprint arXiv:2402.14650*, 2024.
- [14] Wei Cheng, Ruixiang Chen, Siming Fan, Wanqi Yin, Keyu Chen, Zhongang Cai, Jingbo Wang, Yang Gao, Zhengming Yu, Zhengyu Lin, Daxuan Ren, Lei Yang, Ziwei Liu, Chen Change Loy, Chen Qian, Wayne Wu, Dahua Lin, Bo Dai, and Kwan-Yee Lin. Dna-rendering: A diverse neural actor repository for high-fidelity human-centric rendering. In *IEEE/CVF International Conference on Computer Vision, ICCV 2023, Paris, France, October 1-6, 2023*, pages 19925–19936. IEEE, 2023.
- [15] Junting Dong, Qi Fang, Tianshuo Yang, Qing Shuai, Chengyu Qiao, and Sida Peng. ivs-net: Learning human view synthesis from internet videos. In *IEEE/CVF International Conference on Computer Vision, ICCV 2023, Paris, France, October 1-6, 2023*, pages 22885–22894. IEEE, 2023.

- [16] Zijian Dong, Chen Guo, Jie Song, Xu Chen, Andreas Geiger, and Otmar Hilliges. PINA: learning a personalized implicit neural avatar from a single RGB-D video sequence. In *IEEE/CVF Conference on Computer Vision and Pattern Recognition, CVPR 2022, New Orleans, LA, USA, June 18-24, 2022*, pages 20438–20448. IEEE, 2022.
- [17] Qi Fang, Qing Shuai, Junting Dong, Hujun Bao, and Xiaowei Zhou. Reconstructing 3d human pose by watching humans in the mirror. In *CVPR*, 2021.
- [18] Xiangjun Gao, Jiaolong Yang, Jongyoo Kim, Sida Peng, Zicheng Liu, and Xin Tong. Mps-nerf: Generalizable 3d human rendering from multiview images. *CoRR*, abs/2203.16875, 2022.
- [19] Chen Geng, Sida Peng, Zhen Xu, Hujun Bao, and Xiaowei Zhou. Learning neural volumetric representations of dynamic humans in minutes. In *IEEE/CVF Conference on Computer Vision and Pattern Recognition, CVPR 2023, Vancouver, BC, Canada, June 17-24, 2023*, pages 8759–8770. IEEE, 2023.
- [20] Chen Guo, Tianjian Jiang, Xu Chen, Jie Song, and Otmar Hilliges. Vid2avatar: 3d avatar reconstruction from videos in the wild via self-supervised scene decomposition. In *IEEE/CVF Conference on Computer Vision and Pattern Recognition, CVPR 2023, Vancouver, BC, Canada, June 17-24, 2023*, pages 12858–12868. IEEE, 2023.
- [21] Marc Habermann, Lingjie Liu, Weipeng Xu, Michael Zollhöfer, Gerard Pons-Moll, and Christian Theobalt. Real-time deep dynamic characters. *ACM Trans. Graph.*, 40(4):94:1–94:16, 2021.
- [22] Tong He, John P. Collomosse, Hailin Jin, and Stefano Soatto. Geo-pifu: Geometry and pixel aligned implicit functions for single-view human reconstruction. In Hugo Larochelle, Marc’Aurelio Ranzato, Raia Hadsell, Maria-Florina Balcan, and Hsuan-Tien Lin, editors, *Advances in Neural Information Processing Systems 33: Annual Conference on Neural Information Processing Systems 2020, NeurIPS 2020, December 6-12, 2020, virtual*, 2020.
- [23] Fangzhou Hong, Zhaoxi Chen, Yushi Lan, Liang Pan, and Ziwei Liu. Eva3d: Compositional 3d human generation from 2d image collections. *arXiv preprint arXiv:2210.04888*, 2022.
- [24] Shoukang Hu, Fangzhou Hong, Tao Hu, Liang Pan, Haiyi Mei, Weiye Xiao, Lei Yang, and Ziwei Liu. Humanliff: Layer-wise 3d human generation with diffusion model. *arXiv preprint arXiv:2308.09712*, 2023.
- [25] Shoukang Hu, Fangzhou Hong, Liang Pan, Haiyi Mei, Lei Yang, and Ziwei Liu. SHERF: generalizable human nerf from a single image. In *IEEE/CVF International Conference on Computer Vision, ICCV 2023, Paris, France, October 1-6, 2023*, pages 9318–9330. IEEE, 2023.
- [26] Shoukang Hu and Ziwei Liu. Gauhuman: Articulated gaussian splatting from monocular human videos. *CoRR*, abs/2312.02973, 2023.
- [27] Zihao Huang, Min Shi, Chengxin Liu, Ke Xian, and Zhiguo Cao. Simhmr: A simple query-based framework for parameterized human mesh reconstruction. In Abdulmotaleb El-Saddik, Tao Mei, Rita Cucchiara, Marco Bertini, Diana Patricia Tobon Vallejo, Pradeep K. Atrey, and M. Shamim Hossain, editors, *Proceedings of the 31st ACM International Conference on Multimedia, MM 2023, Ottawa, ON, Canada, 29 October 2023- 3 November 2023*, pages 6918–6927. ACM, 2023.
- [28] Catalin Ionescu, Dragos Papava, Vlad Olaru, and Cristian Sminchisescu. Human3.6m: Large scale datasets and predictive methods for 3d human sensing in natural environments. *IEEE Trans. Pattern Anal. Mach. Intell.*, 36(7):1325–1339, 2014.
- [29] Mustafa Isik, Martin Rünz, Markos Georgopoulos, Taras Khakhulin, Jonathan Starck, Lourdes Agapito, and Matthias Nießner. Humanrf: High-fidelity neural radiance fields for humans in motion. *ACM Trans. Graph.*, 42(4):160:1–160:12, 2023.
- [30] Yasamin Jafarian and Hyun Soo Park. Learning high fidelity depths of dressed humans by watching social media dance videos. In *IEEE Conference on Computer Vision and Pattern Recognition, CVPR 2021, virtual, June 19-25, 2021*, pages 12753–12762. Computer Vision Foundation / IEEE, 2021.
- [31] Wei Jiang, Kwang Moo Yi, Golnoosh Samei, Oncel Tuzel, and Anurag Ranjan. Neuman: Neural human radiance field from a single video. In Shai Avidan, Gabriel J. Brostow, Moustapha Cissé, Giovanni Maria Farinella, and Tal Hassner, editors, *Computer Vision - ECCV 2022 - 17th European Conference, Tel Aviv, Israel, October 23-27, 2022, Proceedings, Part XXXII*, volume 13692 of *Lecture Notes in Computer Science*, pages 402–418. Springer, 2022.

- [32] Hanbyul Joo, Natalia Neverova, and Andrea Vedaldi. Exemplar fine-tuning for 3d human model fitting towards in-the-wild 3d human pose estimation. In *Proc. Int. Conf. 3D Vis.*, pages 42–52. Computer Vision Foundation / IEEE, 2021.
- [33] Angjoo Kanazawa, Michael J. Black, David W. Jacobs, and Jitendra Malik. End-to-end recovery of human shape and pose. In *Proc. IEEE Conf. Comput. Vis. Patt. Recogn.*, pages 7122–7131. Computer Vision Foundation / IEEE, 2018.
- [34] Alexander Kirillov, Eric Mintun, Nikhila Ravi, Hanzi Mao, Chloe Rolland, Laura Gustafson, Tete Xiao, Spencer Whitehead, Alexander C. Berg, Wan-Yen Lo, Piotr Dollár, and Ross Girshick. Segment anything. *arXiv:2304.02643*, 2023.
- [35] Muhammed Kocabas, Nikos Athanasiou, and Michael J. Black. VIBE: video inference for human body pose and shape estimation. In *Proc. IEEE Conf. Comput. Vis. Patt. Recogn.*, pages 5252–5262. Computer Vision Foundation / IEEE, 2020.
- [36] Muhammed Kocabas, Chun-Hao P. Huang, Otmar Hilliges, and Michael J. Black. PARE: part attention regressor for 3d human body estimation. In *Proc. IEEE Int. Conf. Comput. Vis.*, pages 11107–11117. Computer Vision Foundation / IEEE, 2021.
- [37] Nikos Kolotouros, Georgios Pavlakos, Michael J. Black, and Kostas Daniilidis. Learning to reconstruct 3d human pose and shape via model-fitting in the loop. In *Proc. IEEE Int. Conf. Comput. Vis.*, pages 2252–2261. Computer Vision Foundation / IEEE, 2019.
- [38] Youngjoong Kwon, Dahun Kim, Duygu Ceylan, and Henry Fuchs. Neural human performer: Learning generalizable radiance fields for human performance rendering. In Marc’Aurelio Ranzato, Alina Beygelzimer, Yann N. Dauphin, Percy Liang, and Jennifer Wortman Vaughan, editors, *Advances in Neural Information Processing Systems 34: Annual Conference on Neural Information Processing Systems 2021, NeurIPS 2021, December 6-14, 2021, virtual*, pages 24741–24752, 2021.
- [39] Ruilong Li, Yuliang Xiu, Shunsuke Saito, Zeng Huang, Kyle Olszewski, and Hao Li. Monocular real-time volumetric performance capture. In Andrea Vedaldi, Horst Bischof, Thomas Brox, and Jan-Michael Frahm, editors, *Computer Vision - ECCV 2020 - 16th European Conference, Glasgow, UK, August 23-28, 2020, Proceedings, Part XXIII*, volume 12368 of *Lecture Notes in Computer Science*, pages 49–67. Springer, 2020.
- [40] Zhe Li, Tao Yu, Zerong Zheng, and Yebin Liu. Robust and accurate 3d self-portraits in seconds. *IEEE Trans. Pattern Anal. Mach. Intell.*, 44(11):7854–7870, 2022.
- [41] Zhihao Li, Jianzhuang Liu, Zhensong Zhang, Songcen Xu, and Youliang Yan. CLIFF: carrying location information in full frames into human pose and shape estimation. In Shai Avidan, Gabriel J. Brostow, Moustapha Cissé, Giovanni Maria Farinella, and Tal Hassner, editors, *Proc. Eur. Conf. Comput. Vis.*, volume 13665 of *Lecture Notes in Computer Science*, pages 590–606. Springer-Verlag, 2022.
- [42] Haotong Lin, Sida Peng, Zhen Xu, Yunzhi Yan, Qing Shuai, Hujun Bao, and Xiaowei Zhou. Efficient neural radiance fields for interactive free-viewpoint video. In Soon Ki Jung, Jehee Lee, and Adam W. Bargteil, editors, *SIGGRAPH Asia 2022 Conference Papers, SA 2022, Daegu, Republic of Korea, December 6-9, 2022*, pages 39:1–39:9. ACM, 2022.
- [43] Jing Lin, Ailing Zeng, Shunlin Lu, Yuanhao Cai, Ruimao Zhang, Haoqian Wang, and Lei Zhang. Motion-x: A large-scale 3d expressive whole-body human motion dataset. In Alice Oh, Tristan Naumann, Amir Globerson, Kate Saenko, Moritz Hardt, and Sergey Levine, editors, *Advances in Neural Information Processing Systems 36: Annual Conference on Neural Information Processing Systems 2023, NeurIPS 2023, New Orleans, LA, USA, December 10 - 16, 2023*, 2023.
- [44] Shanchuan Lin, Andrey Ryabtsev, Soumyadip Sengupta, Brian L. Curless, Steven M. Seitz, and Ira Kemelmacher-Shlizerman. Real-time high-resolution background matting. In *IEEE Conference on Computer Vision and Pattern Recognition, CVPR 2021, virtual, June 19-25, 2021*, pages 8762–8771. Computer Vision Foundation / IEEE, 2021.
- [45] Tianqi Liu, Guangcong Wang, Shoukang Hu, Liao Shen, Xinyi Ye, Yuhang Zang, Zhiguo Cao, Wei Li, and Ziwei Liu. Fast generalizable gaussian splatting reconstruction from multi-view stereo. *arXiv preprint arXiv:2405.12218*, 2024.

- [46] Xian Liu, Xiaohang Zhan, Jiayang Tang, Ying Shan, Gang Zeng, Dahua Lin, Xihui Liu, and Ziwei Liu. Humangaussian: Text-driven 3d human generation with gaussian splatting. *arXiv preprint arXiv:2311.17061*, 2023.
- [47] Matthew Loper, Naureen Mahmood, Javier Romero, Gerard Pons-Moll, and Michael J. Black. SMPL: a skinned multi-person linear model. *ACM Trans. Graph.*, 34(6):248:1–248:16, 2015.
- [48] Dushyant Mehta, Helge Rhodin, Dan Casas, Pascal Fua, Oleksandr Sotnychenko, Weipeng Xu, and Christian Theobalt. Monocular 3d human pose estimation in the wild using improved CNN supervision. In *Proc. Int. Conf. 3D Vis.*, pages 506–516. Computer Vision Foundation / IEEE, 2017.
- [49] Ben Mildenhall, Pratul P Srinivasan, Matthew Tancik, Jonathan T Barron, Ravi Ramamoorthi, and Ren Ng. Nerf: Representing scenes as neural radiance fields for view synthesis. *Communications of the ACM*, 65(1):99–106, 2021.
- [50] Georgios Pavlakos, Vasileios Choutas, Nima Ghorbani, Timo Bolkart, Ahmed A. A. Osman, Dimitrios Tzionas, and Michael J. Black. Expressive body capture: 3d hands, face, and body from a single image. In *Proc. IEEE Conf. Comput. Vis. Patt. Recogn.*, pages 10975–10985. Computer Vision Foundation / IEEE, 2019.
- [51] Sida Peng, Junting Dong, Qianqian Wang, Shangzhan Zhang, Qing Shuai, Xiaowei Zhou, and Hujun Bao. Animatable neural radiance fields for modeling dynamic human bodies. In *ICCV*, 2021.
- [52] Sida Peng, Zhen Xu, Junting Dong, Qianqian Wang, Shangzhan Zhang, Qing Shuai, Hujun Bao, and Xiaowei Zhou. Animatable implicit neural representations for creating realistic avatars from videos. *TPAMI*, 2024.
- [53] Sida Peng, Yuanqing Zhang, Yinghao Xu, Qianqian Wang, Qing Shuai, Hujun Bao, and Xiaowei Zhou. Neural body: Implicit neural representations with structured latent codes for novel view synthesis of dynamic humans. In *Proc. IEEE Conf. Comput. Vis. Patt. Recogn.*, pages 9054–9063. Computer Vision Foundation / IEEE, 2021.
- [54] Pavlin G. Policar and Blaz Zupan. Visualizing high-dimensional temporal data using direction-aware t-sne. *CoRR*, abs/2403.19040, 2024.
- [55] Joseph Redmon, Santosh Kumar Divvala, Ross B. Girshick, and Ali Farhadi. You only look once: Unified, real-time object detection. In *2016 IEEE Conference on Computer Vision and Pattern Recognition, CVPR 2016, Las Vegas, NV, USA, June 27-30, 2016*, pages 779–788. IEEE Computer Society, 2016.
- [56] Renderpeople. Renderpeople, 2018. <https://renderpeople.com/3d-people>.
- [57] Javier Romero, Dimitrios Tzionas, and Michael J. Black. Embodied hands: Modeling and capturing hands and bodies together. *CoRR*, abs/2201.02610, 2022.
- [58] Shunsuke Saito, Zeng Huang, Ryota Natsume, Shigeo Morishima, Hao Li, and Angjoo Kanazawa. Pifu: Pixel-aligned implicit function for high-resolution clothed human digitization. In *Proc. IEEE Int. Conf. Comput. Vis.*, pages 2304–2314. Computer Vision Foundation / IEEE, 2019.
- [59] Shunsuke Saito, Tomas Simon, Jason M. Saragih, and Hanbyul Joo. Pifuhd: Multi-level pixel-aligned implicit function for high-resolution 3d human digitization. In *Proc. IEEE Conf. Comput. Vis. Patt. Recogn.*, pages 81–90. Computer Vision Foundation / IEEE, 2020.
- [60] Umme Sara, Morium Akter, and Mohammad Shorif Uddin. Image quality assessment through fsim, ssim, mse and psnr—a comparative study. *Journal of Computer and Communications*, page 8–18, Jan 2019.
- [61] M. Schmidt. minfunc: unconstrained differentiable multivariate optimization in matlab. 2005.
- [62] Ruizhi Shao, Zerong Zheng, Hongwen Zhang, Jingxiang Sun, and Yebin Liu. Diffustereo: High quality human reconstruction via diffusion-based stereo using sparse cameras. In *ECCV*, 2022.
- [63] Zhaoqi Su, Tao Yu, Yangang Wang, and Yebin Liu. Deepcloth: Neural garment representation for shape and style editing. *IEEE Transactions on Pattern Analysis and Machine Intelligence*, 45(2):1581–1593, 2023.
- [64] Ke Sun, Bin Xiao, Dong Liu, and Jingdong Wang. Deep high-resolution representation learning for human pose estimation. In *Proc. IEEE Conf. Comput. Vis. Patt. Recogn.*, pages 5693–5703. Computer Vision Foundation / IEEE, 2019.

- [65] Yu Sun, Qian Bao, Wu Liu, Yili Fu, Michael J. Black, and Tao Mei. Monocular, one-stage, regression of multiple 3d people. In *Proc. IEEE Int. Conf. Comput. Vis.*, pages 11159–11168. Computer Vision Foundation / IEEE, 2021.
- [66] Ayush Tewari, Justus Thies, Ben Mildenhall, Pratul P. Srinivasan, Edgar Tretschk, Yifan Wang, Christoph Lassner, Vincent Sitzmann, Ricardo Martin-Brualla, Stephen Lombardi, Tomas Simon, Christian Theobalt, Matthias Nießner, Jonathan T. Barron, Gordon Wetzstein, Michael Zollhöfer, and Vladislav Golyanik. Advances in neural rendering. *Comput. Graph. Forum*, 41(2):703–735, 2022.
- [67] Shuhei Tsuchida, Satoru Fukayama, Masahiro Hamasaki, and Masataka Goto. AIST dance video database: Multi-genre, multi-dancer, and multi-camera database for dance information processing. In Arthur Flexer, Geoffroy Peeters, Julián Urbano, and Anja Volk, editors, *Proceedings of the 20th International Society for Music Information Retrieval Conference, ISMIR 2019, Delft, The Netherlands, November 4-8, 2019*, pages 501–510, 2019.
- [68] Timo von Marcard, Roberto Henschel, Michael J. Black, Bodo Rosenhahn, and Gerard Pons-Moll. Recovering accurate 3d human pose in the wild using imus and a moving camera. In Vittorio Ferrari, Martial Hebert, Cristian Sminchisescu, and Yair Weiss, editors, *Proc. Eur. Conf. Comput. Vis.*, volume 11214 of *Lecture Notes in Computer Science*, pages 614–631. Springer-Verlag, 2018.
- [69] Jiong Wang, Fengyu Yang, Wenbo Gou, Bingliang Li, Danqi Yan, Ailing Zeng, Yijun Gao, Junle Wang, and Ruimao Zhang. Freeman: Towards benchmarking 3d human pose estimation in the wild. *CoRR*, abs/2309.05073, 2023.
- [70] Tengfei Wang, Bo Zhang, Ting Zhang, Shuyang Gu, Jianmin Bao, Tadas Baltrusaitis, Jingjing Shen, Dong Chen, Fang Wen, Qifeng Chen, et al. Rodin: A generative model for sculpting 3d digital avatars using diffusion. In *Proceedings of the IEEE/CVF conference on computer vision and pattern recognition*, pages 4563–4573, 2023.
- [71] Zhou Wang, Alan C. Bovik, Hamid R. Sheikh, and Eero P. Simoncelli. Image quality assessment: from error visibility to structural similarity. *IEEE Trans. Image Process.*, 13(4):600–612, 2004.
- [72] Chung-Yi Weng, Brian Curless, Pratul P. Srinivasan, Jonathan T. Barron, and Ira Kemelmacher-Shlizerman. Humannerf: Free-viewpoint rendering of moving people from monocular video. In *Proc. IEEE Conf. Comput. Vis. Patt. Recogn.*, pages 16189–16199. Computer Vision Foundation / IEEE, 2022.
- [73] Minye Wu, Yuehao Wang, Qiang Hu, and Jingyi Yu. Multi-view neural human rendering. In *2020 IEEE/CVF Conference on Computer Vision and Pattern Recognition, CVPR 2020, Seattle, WA, USA, June 13-19, 2020*, pages 1679–1688. Computer Vision Foundation / IEEE, 2020.
- [74] Hongyi Xu, Eduard Gabriel Bazavan, Andrei Zanfir, William T. Freeman, Rahul Sukthankar, and Cristian Sminchisescu. GHUM & GHUML: generative 3d human shape and articulated pose models. In *Proc. IEEE Conf. Comput. Vis. Patt. Recogn.*, pages 6183–6192. Computer Vision Foundation / IEEE, 2020.
- [75] Ze Yang, Shenlong Wang, Sivabalan Manivasagam, Zeng Huang, Wei-Chiu Ma, Xinchun Yan, Ersin Yumer, and Raquel Urtasun. S3: neural shape, skeleton, and skinning fields for 3d human modeling. In *IEEE Conference on Computer Vision and Pattern Recognition, CVPR 2021, virtual, June 19-25, 2021*, pages 13284–13293. Computer Vision Foundation / IEEE, 2021.
- [76] Yifei Yin, Chen Guo, Manuel Kaufmann, Juan Jose Zarate, Jie Song, and Otmar Hilliges. Hi4d: 4d instance segmentation of close human interaction. In *IEEE/CVF Conference on Computer Vision and Pattern Recognition, CVPR 2023, Vancouver, BC, Canada, June 17-24, 2023*, pages 17016–17027. IEEE, 2023.
- [77] Jae Shin Yoon, Zhixuan Yu, Jaesik Park, and Hyun Soo Park. HUMBI: A large multiview dataset of human body expressions and benchmark challenge. *IEEE Trans. Pattern Anal. Mach. Intell.*, 45(1):623–640, 2023.
- [78] Tao Yu, Zerong Zheng, Kaiwen Guo, Pengpeng Liu, Qionghai Dai, and Yebin Liu. Function4d: Real-time human volumetric capture from very sparse consumer rgbd sensors. In *IEEE Conference on Computer Vision and Pattern Recognition (CVPR2021)*, June 2021.
- [79] Hongwen Zhang, Yating Tian, Xinchun Zhou, Wanli Ouyang, Yebin Liu, Limin Wang, and Zhenan Sun. Pymaf: 3d human pose and shape regression with pyramidal mesh alignment

- feedback loop. In *Proc. IEEE Int. Conf. Comput. Vis.*, pages 11426–11436. Computer Vision Foundation / IEEE, 2021.
- [80] Richard Zhang, Phillip Isola, Alexei A. Efros, Eli Shechtman, and Oliver Wang. The unreasonable effectiveness of deep features as a perceptual metric. In *2018 IEEE Conference on Computer Vision and Pattern Recognition, CVPR 2018, Salt Lake City, UT, USA, June 18-22, 2018*, pages 586–595. Computer Vision Foundation / IEEE Computer Society, 2018.
 - [81] Yuxiang Zhang, Zhe Li, Liang An, Mengcheng Li, Tao Yu, and Yebin Liu. Light-weight multi-person total capture using sparse multi-view cameras. In *IEEE International Conference on Computer Vision*, 2021.
 - [82] Xiaoyun Zheng, Liwei Liao, Xufeng Li, Jianbo Jiao, Rongjie Wang, Feng Gao, Shiqi Wang, and Ronggang Wang. Pku-dymvhums: A multi-view video benchmark for high-fidelity dynamic human modeling. *CoRR*, abs/2403.16080, 2024.
 - [83] Zerong Zheng, Han Huang, Tao Yu, Hongwen Zhang, Yandong Guo, and Yebin Liu. Structured local radiance fields for human avatar modeling. In *Proceedings of the IEEE/CVF Conference on Computer Vision and Pattern Recognition (CVPR)*, June 2022.
 - [84] Zerong Zheng, Tao Yu, Yixuan Wei, Qionghai Dai, and Yebin Liu. Deephuman: 3d human reconstruction from a single image. In *2019 IEEE/CVF International Conference on Computer Vision, ICCV 2019, Seoul, Korea (South), October 27 - November 2, 2019*, pages 7738–7748. IEEE, 2019.
 - [85] Taotao Zhou, Kai He, Di Wu, Teng Xu, Qixuan Zhang, Kuixiang Shao, Wenzheng Chen, Lan Xu, and Jingyi Yu. Relightable neural human assets from multi-view gradient illuminations. In *IEEE/CVF Conference on Computer Vision and Pattern Recognition, CVPR 2023, Vancouver, BC, Canada, June 17-24, 2023*, pages 4315–4327. IEEE, 2023.

A Details in Data Pipeline

We provide more details on the data processing pipeline in addition to the main paper.

Stage I: Human Bounding Box Detection and Tracking. We first obtain the bounding box of human subjects with an off-the-shelf state-of-the-art Yolo detection method [55]². We only keep the video clip with at least one “person” instance with its detection threshold over 0.8. The tracking step is based on finding the largest IOU overlay of bounding boxes among frames. We discard low-resolution human subjects whose bounding box areas are lower than 64×64 . To ensure the richness of the dataset, we only keep one “key subject” for each video, as clips of the same video may probably share the same key subject.

Stage II: Human Segmentation Mask Extraction. To prepare key point exemplars for the *Segment Anything*, we first obtain the 2D keypoints J_{2D} for human subjects using the popular HRNet [64]³. Given the 2D keypoint annotations, we are also able to discard over part-occluded subjects. Specially, we only keep the subject with the average confidence of 2D keypoints over 0.45. For segmentation, we feed the 2D bounding box and the 2D keypoints into the *sam_vit_h* sub-model to extract the foreground mask.

Stage III: Coarse SMPL and Camera Estimation. We first estimate SMPL and camera parameters frame by frame, using a state-of-the-art single-image-based human pose and shape estimation method PARE [36]. To achieve better performance in complex scenes in the wild, we adapt the model pre-trained on the in-the-wild 3DPW dataset [68]. The PARE infers human body pose/shape parameters (θ/β) , and the global camera parameters (rotation matrix R and the 3D offset T).

To retain the remaining video clips with considerable viewpoint shifts and human movements, we discard the clips with viewpoint angle changes lower than $\frac{\pi}{4}$ *rad*. And we automatically select $N = 20$ most non-trivial frames, which keep the pose diversity to the greatest extent possible.

As mentioned in the main paper, we double-check the consistency between the SAM masks and the SMPL masks. Intuitively, the SMPL mask denotes the naked body, while the SAM mask contains the clothed body. Therefore, the SMPL mask should be mostly covered by the SAM mask (See Fig. A1 (a) ~ (d)). We discard the subjects whose SAM masks are over $3 \times$ larger than their SMPL masks (See Fig. A1 (e) ~ (h)). We also discard the subjects whose 10% SMPL mask pixels are not covered by the SAM mask (See Fig. A1 (i) ~ (l)).

Stage IV: Refining SMPL and Camera In-the-loop. For high-quality annotations, here we refine the coarse SMPL parameters (θ, β) and camera parameters (R, T) obtained in Stage I. To achieve temporally smooth results, we regularize the differences in parameters between adjacent frames, which is given by

$$\begin{aligned} \mathcal{L}_\theta^s &= \sum_{i=1}^{N-1} \|\theta^i - \theta^{i+1}\|_2, \mathcal{L}_R^s = \sum_{i=1}^{N-1} \|R^i - R^{i+1}\|_2, \mathcal{L}_T^s = \sum_{i=1}^{N-1} \|T^i - T^{i+1}\|_2, \\ \mathcal{L}_{2D}^s &= \sum_{i=1}^{N-1} \|\Pi(J_{3D}(\theta^i, \beta^i); R^i, T^i) - \Pi(J_{3D}(\theta^{i+1}, \beta^{i+1}); R^{i+1}, T^{i+1})\|_2, \end{aligned} \quad (1)$$

where $J_{3D}(\theta, \beta)$ infers the 3D keypoints of the human body, and the Π denotes the 2D projection, and i denotes the i_{th} frame of the input video. Notice that the body shapes (β) are treated as constants across the input video.

In addition, we align the human body parameters to the 2D keypoints and SAM masks, which are given by

$$\mathcal{L}_{2D} = \sum_{i=1}^N \|\Pi(J_{3D}(\theta^i, \beta^i)) - J_{2D}^i\|_2, \mathcal{L}_{\text{mask}} = \sum_{i=1}^N d_{CD}(\Pi(V_{3D}(\theta^i, \beta^i)), M^i), \quad (2)$$

where d_{CD} denotes the chamfer distance between point clouds, and the $V_{3D}(\theta, \beta)$ infers the 3D vertex of the human body. The M^i denotes the foreground d pixels cloud of the i frame. We also

²The configuration of the detection model can be found [here](#).

³The configuration of the 2D keypoint estimation model can be found [here](#).

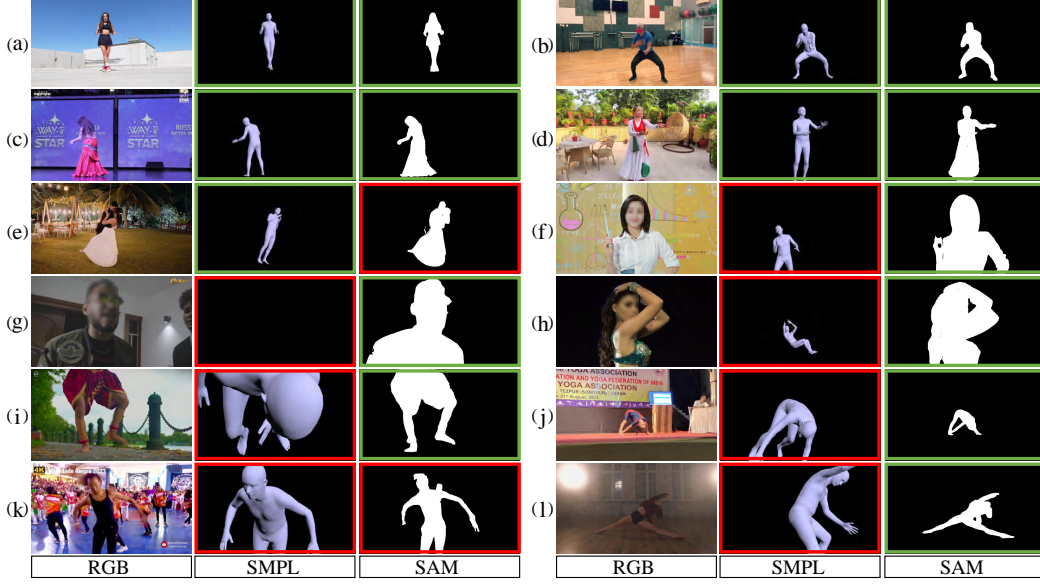


Figure A1: SMPL and SAM consistency. The green/red borders denote good/bad outputs, respectively.

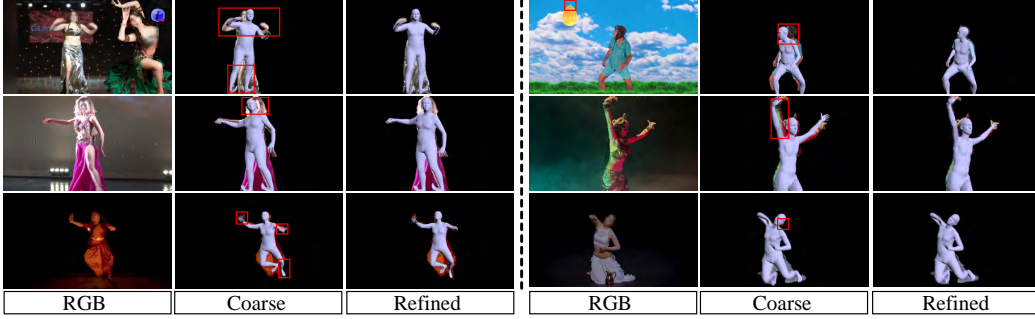


Figure A2: Comparison of the coarse and refined SMPL parameters.

regularize θ to avoid out-of-domain poses [7], using the Gaussian Mixture Model (GMM) prior [50]

$$\mathcal{L}_{\text{prior}} = \sum_{i=1}^N \|GMM(\theta^i)\|_2. \quad (3)$$

We adopt the loss functions as mentioned above for supervision:

$$\begin{aligned} \mathcal{L} = & \lambda_{\theta}^s \mathcal{L}_{\theta}^s + \lambda_R^s \mathcal{L}_R^s + \lambda_T^s \mathcal{L}_T^s + \lambda_{2D}^s \mathcal{L}_{2D}^s \\ & + \lambda_{2D} \mathcal{L}_{2D} + \lambda_{\text{mask}} \mathcal{L}_{\text{mask}} + \lambda_{\text{prior}} \mathcal{L}_{\text{prior}}. \end{aligned} \quad (4)$$

We empirically set the loss weights as $\lambda_{\theta}^s = 100$, $\lambda_R^s = 1000$, $\lambda_T^s = 50$, $\lambda_{2D}^s = 100$, $\lambda_{2D} = 100$, $\lambda_{\text{mask}} = 100$ and $\lambda_{\text{prior}} = 0.1$. We adopt the LBFGS [61] optimizer with the learning rate $lr = 1.0$. We optimize for 20 steps on a single Geforce GTX 1080Ti GPU.

Qualitative comparisons between coarse and refined SMPL and camera parameters can be found in Fig. A2.

B Additional Links

We release the WildAvatar dataset with a permanent doi [10.5281/zenodo.11526806](https://doi.org/10.5281/zenodo.11526806). We also provide the [Croissant metadata](#). The authors bear all responsibility in case of violation of rights, and confirm that this dataset is open-sourced under the [CC BY 4.0 International license](#).